

Exploration of LiCoO₂-doped cobalt oxide composite for thermochemical energy storage at high temperature

Rongjun Wu ^a, Lisheng Deng ^b, Hongyu Huang ^b, Mitsuhiro Kubota ^a, Noriyuki Kobayashi ^{a,*}

^a Department of Chemical Systems Engineering, Graduate School of Engineering, Nagoya University, Furo-cho, Chikusa-ku, Nagoya-shi, Aichi 464-8603, Japan

^b Guangzhou Institute of Energy Conversion, Chinese Academy of Sciences, No. 2 Nengyuan Road, Wushan, Tianhe District, Guangzhou 510640, China

ARTICLE INFO

Keywords:

Thermochemical energy storage
Reduction/oxidation process
Cobalt oxide
Lithium compound dopant
Cyclic stability

ABSTRACT

Due to the high energy storage density, long-term energy storage and long-distance transport possibility, as well as operation possibility under open system, metal oxide-based thermochemical energy storage (TCS) was considered as a promising candidate for efficient energy utilization. Herein, lithium cobalt oxide (LiCoO₂)-doped cobalt oxide composite was proposed and investigated for the metal oxide-based TCS application. Doping with LiCoO₂ diminished the onset temperature of reduction and re-oxidation by 50 °C and 65 °C, respectively. Also, doping with appropriate amount of LiCoO₂ contributed to improve the re-oxidation rate of cobalt oxide-based system under a high cooling rate, resulting the discharging heat (423.8 kJ/kg) increased significantly in comparison with pure cobalt oxide (289.8 kJ/kg) under temperature cooling rate of 20 °C/min. It was found that doping with LiCoO₂ decreased the apparent activation energy of reduction and oxidation. Meanwhile, the results obtained from in-situ X-ray diffraction indicate that LiCoO₂ was involved in the reduction/re-oxidation process. Moreover, excellent repeatability of the composite was attested in 30 cycles. Hence, doping with LiCoO₂ was verified as an effective method to expanding the possibility of cobalt oxide for TCS application.

1. Introduction

With the consistent growth of energy consumption, developing efficient energy utilization technology becomes an attractive subject in the globe. Thermal energy storage technology is becoming increasingly important to realize the efficient use of energy [1,2]. Generally, thermal energy storage technologies can be classified into three categories: sensible heat storage system, latent heat storage system and thermochemical energy storage (TCS) system. Compared with sensible and latent heat storage systems, thermochemical energy storage system, which can store and release thermal energy through reversible chemical reaction, possesses the following advantages: high energy storage density, energy storage at room temperature, long-term energy storage and long-distance transport possibility [3–5]. Metal oxide-based TCS system is based on reversible reduction and oxidation of metal oxides. In reduction process, thermal energy is used to drive the endothermic reduction of metal oxide along with oxygen release. In the reverse oxidation process, thermal energy is released through the exothermic oxidation of metal oxide along with oxygen uptake. This system can be performed in an open-loop plant where air is used as the source of oxygen as well as the thermal energy transfer medium [6]. Hence, there are

no technical requirements for gas separation and storage in comparison with other TCS systems, such as CO₂ separation and storage for carbonate-based TCS system, and H₂O storage for hydroxide-based TCS system. In recent years, metal oxide-based TCS was mainly studied for the concentrating solar power (CSP) plants. In a typical process, high-temperature air heated by solar energy is employed to drive the reduction of metal oxide, simultaneously partial thermal energy is stored in the reduced metal oxide. Then, the reduced metal oxide is cooled down under oxygen-poor condition. During the night time or on rainy day, the thermal energy can be released by oxidizing the reduced metal oxide with air [4].

In the last over 40 years, scientists have donated considerable efforts to explore suitable and efficient materials for metal oxide-based TCS application. In terms of conventional metal oxides, BaO₂/BaO [7], Co₃O₄/CoO [8–12], Mn₂O₃/Mn₃O₄ [12,13], and CuO/Cu₂O [14] pairs were proposed as promising candidates for TCS application. Recently, several novel multi-metal oxides exhibited the potential in TCS application like perovskite oxides [15–18], iron-manganese oxides [19–24], copper-manganese oxides [23,24], lithium-manganese oxides [25,26]. Among them, cobalt oxide (Co₃O₄/CoO), which has high energy storage density and remarkable recyclability in the temperature range of

* Corresponding author.

E-mail address: kobayashi.noriyuki@material.nagoya-u.ac.jp (N. Kobayashi).

870–955 °C in air [8–10], was considered as one of the most attractive candidates for metal oxide-based TCS application. Cobalt oxide as well as other Co-based materials played significant roles in various fields [27]. For instance, cobalt was used in the Li-ion batteries as a vital element [28]. Cobalt-based materials were employed as catalysts for several reactions like hydrogen evolution reaction [29]. Cobalt can exhibit multiple oxidation states (Co^{2+} , Co^{3+} and Co^{4+}), which generates the redox reaction of cobalt oxide. Based on the redox reaction, cobalt oxide was utilized in supercapacitor for charging storage [30]. Moreover, cobalt oxide was proposed for oxygen production [8]. The possible utilization of cobalt oxide for TCS was emphasized in the project led by the American company General Atomics, in collaboration with DLR, from which a growing number of researches concerning TCS focused on the cobalt oxide [31]. The redox process is showed in the following equation:



where the right side in Eq. (1), Co_3O_4 reduction, is an endothermic step corresponding to thermal energy storage, and the left side, CoO oxidation, is an exothermic step corresponding to thermal energy release.

To improve the chemical properties and parameters of $\text{Co}_3\text{O}_4/\text{CoO}$ redox process for TCS practical application, several researches based on cobalt oxide system have been done, such as coating Co_3O_4 on porous ceramic structures [10], shaping Co_3O_4 into porous structures [11], as well as modified cobalt oxide by doping with other metal cations. Suitable amount of Fe was found to be beneficial for the microstructural stability [24,32]. Doping with Mn, Ni, Cu and Mg did not show better redox performance than pure cobalt oxide [9,24,33]. Nevertheless, some researches have reported that Ni-doping [34] and Cu-doping [24] can help to lower the working temperature, which make it possible to use cobalt oxide-based system in applications for lower temperature.

To broaden the working temperature and widen more applicability of cobalt oxide-based system for TCS application, this work proposed a cobalt oxide-based composite, which is composed of lithium cobalt oxide (LiCoO_2) and cobalt oxide. LiCoO_2 has been widely used for lithium-ion batteries. The basic reaction of LiCoO_2 in a lithium-ion battery is well known to be lithium ion extraction from or insertion into a layered cobalt dioxide matrix by varying the interlayer distance [35]. Accordingly, LiCoO_2 was exploited as the support of Pt catalyst to control the lattice strain of Pt catalyst and thus to tune the catalytic activity in the oxygen reduction reaction [36]. Besides, LiCoO_2 was also utilized as catalyst for oxygen evolution reaction [37]. It is worthy to mention that lithium compounds were frequently used as an adjuvant or enhancer in several TCS systems [38]. Addition with lithium compounds was found to be beneficial to lower the dehydration temperature, improve the heat output density and enhance the reactivity of reaction process in dehydration/hydration system (i.e. $\text{CaO}/\text{Ca}(\text{OH})_2$ system and $\text{MgO}/\text{Mg}(\text{OH})_2$ system) [39–47]. Addition with lithium compounds also was found to promote the carbonation of MgO/MgCO_3 system [48]. In metal oxide-based TCS system, lithium-manganese oxides were proposed as possible working mediums for TCS application [25,26]. To the best of our knowledge, there were rare researches that reported the effect of doping lithium compounds on metal oxide-based TCS system. In the present work, Co_3O_4 was doped with LiCoO_2 by a simple mixing process to prepare the LiCoO_2 -doped cobalt oxide composite. The redox behavior of this composite was investigated. The optimum doping amount of LiCoO_2 was determined. The repeatability of this composite was also tested. Moreover, the reduction/re-oxidation process of this composite was explored and discussed. Additionally, pure cobalt oxide was used for comparative analysis.

2. Experimental section

2.1. Preparation of samples

Co_3O_4 powder (99.99 %, Kanto Chemical CO., INC.) and LiCoO_2 powder (99.988 %, Toshima Manufacturing CO., Ltd.) were used as received. Certain amount of Co_3O_4 and LiCoO_2 were weighed and put in a mortar. To avoid the deviation generated in the milling process, the total weight of each sample was weighed in around 1000 mg. Materials were carefully mixed by hand, grinding with a speed of ~2 laps per second for 20 min. In this work, samples with different doping amounts of LiCoO_2 were prepared. The molar ratio, x , is defined as,

$$x = \frac{m_{\text{LiCoO}_2}/M_{\text{LiCoO}_2}}{m_{\text{LiCoO}_2}/M_{\text{LiCoO}_2} + m_{\text{Co}_3\text{O}_4}/M_{\text{Co}_3\text{O}_4}} \quad (2)$$

where m_{LiCoO_2} is the weight of LiCoO_2 , and M_{LiCoO_2} is the molecular weight of LiCoO_2 . $m_{\text{Co}_3\text{O}_4}$ is the weight of Co_3O_4 , and $M_{\text{Co}_3\text{O}_4}$ is the molecular weight of Co_3O_4 .

2.2. Characterization

The crystal structure of sample was identified by X-ray diffraction (XRD; Rigaku Ultima IV) with $\text{Cu K}\alpha$ radiation (40 kV/30 mA). The morphology of sample was collected by scanning electronic microscope (SEM; JEOL JSM-7500FA). The composition of sample was measured by inductively coupled plasma optical emission spectrometers (ICP, PerkinElmer OPTIMA 8000DV).

2.3. Redox investigation

The reduction/re-oxidation process of sample was performed by thermogravimetric analyzer (TGA; HITACHI STA7300). In general, reduction and re-oxidation steps were performed in air atmosphere under a constant flow of 200 mL/min. The temperature program consisted of a heating step from 700 °C to 1000 °C with following holding for 5 min and then a cooling step from 1000 °C to 700 °C with following holding for 5 min. Heating/cooling steps were performed with ramping rates of ± 10 °C/min. The temperature program was proceeded in two cycles for eliminating the influences caused by impurity. Also, the repeatability of sample was performed by TGA with appropriate temperature procedures. All samples were weighed in approximately 10 mg. During the reduction process, oxygen released leading to a weight loss of sample. During re-oxidation process, oxygen uptake occurred leading to a weight gain of sample. The weight change, α (%), is defined as,

$$\alpha = \frac{m_i - m_t}{m_i} \times 100 \quad (3)$$

where m_i is the initial weight of sample, and m_t is the weight at time t . Due to the possible impurities existed in samples, initial weight of the second cycle was used as the initial weight for each sample.

Moreover, the conversion ratio of reduction/re-oxidation, β (%), is defined as,

$$\beta = \frac{m_0 - m_t}{m_0 - m_f} \times 100 \quad (4)$$

where m_0 is the initial weight of sample before the reduction/re-oxidation process, m_t is the weight at time t , and m_f is the final weight of sample after the reduction/re-oxidation process.

The apparent activation energy of reduction and oxidation for samples were calculated by isoconversional Friedman method [25,49,50], which is represented by the following equation:

$$\ln \left[i \cdot \left(\frac{d\beta}{dT} \right) \right] = \ln[Af(\beta)] - \frac{E}{RT} \quad (5)$$

where i is the heating rate (K/min), β is the conversion ratio, A is the pre-exponential factor, $f(\beta)$ is the reaction model, E is the apparent activation energy (J/mol), R is the gas constant (8.314 J/K/mol), T is the temperature (K) at which the extent of conversion β is reached under the heat rate i . For each given β , the apparent activation energy E is determined from the slope of the plot of $\ln[i \cdot (d\beta/dT)]$ against $1/T$. The apparent activation energy of reduction was calculated based on the heating rate of 5, 10, 15 and 20 K/min. The apparent activation energy of oxidation was calculated by reduced samples based on the heating rate of 1, 3, 5 and 10 K/min. To obtain reduced samples, the as-prepared samples were heated to 1000 °C in air, and then cooled down to room temperature in nitrogen.

Simultaneous thermogravimetry-differential scanning calorimetry (TG-DSC, NETZSCH STA449F3) was carried out to study the heat charging and discharging during reduction and re-oxidation process. The temperature procedure consisted of a heating step from 30 °C to 1020 °C with following holding for 30 min and then a cooling step from 1020 °C to 100 °C with following holding for 5 min. Both heating and cooling steps were performed in air atmosphere under a constant flow of 100 mL/min with ramping rates of ±20 °C/min.

The reduction/re-oxidation process was analyzed by in-situ X-ray diffraction (in-situ XRD; Rigaku SmartLab 3 kW) with Cu K α radiation (40 kV/40 mA). The powder patterns were recorded during a heating/cooling process between 30 °C and 1000 °C.

3. Results and discussion

3.1. Characterization of samples

The chemical compositions of pure Co₃O₄, pure LiCoO₂ and mixed samples with different molar ratios (x) were confirmed by ICP (Table S1). Fig. 1 shows the XRD patterns of these samples. All mixed samples presented the characteristic reflections of LiCoO₂ phase (PDF: 01-070-2685) and Co₃O₄ phase (PDF: 00-043-1003). No new diffraction peaks were detected after mixing process. Fig. 2 shows the SEM images

of these samples. Each sample shows an agglomerate morphology with terraced structure made of particles. Obviously, different particle sizes can be observed between Co₃O₄ ($\geq 1 \mu\text{m}$) and LiCoO₂ ($\leq 0.5 \mu\text{m}$). Therefore, it is easy to distinguish LiCoO₂ particles from Co₃O₄ particles. As we can see in the images taken from mixed samples, LiCoO₂ particles dispersed on the surface of Co₃O₄. What is more, different amounts of LiCoO₂ particles can be observed. With the increasing of x value, the amount of LiCoO₂ particles increased.

3.2. Redox behaviors of samples

The redox behaviors of samples with different molar ratios (x) were explored. Fig. 3 shows the TGA results of samples with different molar ratios (x). The redox performance of pure LiCoO₂ was also tested. As shown in Fig. 3, there was no reversible reaction occurred for pure LiCoO₂ under the configured temperature program. In terms of mixed samples and pure Co₃O₄, there was an initial weight loss before the rapid weight loss for each sample in the first heating step, which may attribute to two reasons: (1) the absorbed compounds like water, CO₂, and O₂ were irreversibly eliminated; (2) oxygen vacancies were generated in the crystal lattice of metal oxide at elevated temperature (with corresponding loss of oxygen), which caused by point defect [28,51,52]. And then, a rapid weight loss occurred with the increasing temperature from 700 °C to 1000 °C for each sample due to the oxygen release in reduction process. Subsequently, the weight of each sample increased with the decreasing temperature from 1000 °C to 700 °C due to the oxygen uptake in re-oxidation process. Apparently, different redox behaviors with respect to reduction/re-oxidation temperature and weight change can be observed among mixed samples and pure Co₃O₄. The reduction/re-oxidation temperature will be discussed in Figs. 4 and 5. The important matter about reduction/re-oxidation temperature illustrated in Fig. 3 is that the mixed samples exhibited relatively low reduction/re-oxidation temperature in comparison with pure Co₃O₄.

In terms of the weight change, it is clearly visible that the weight change corresponding to the amount of oxygen release/uptake

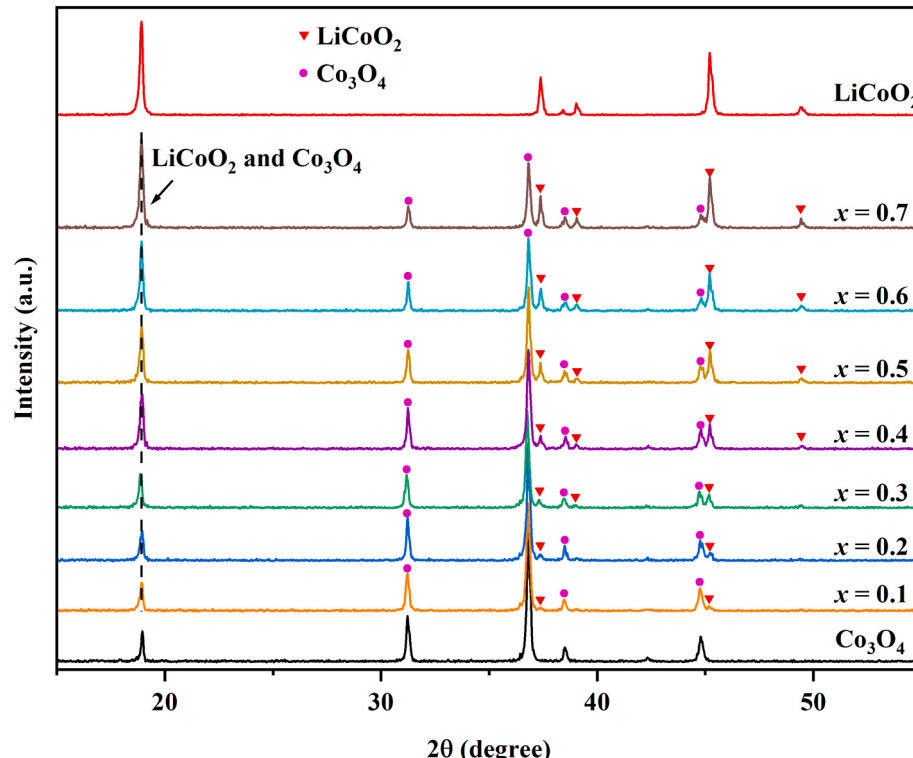


Fig. 1. XRD patterns of Co₃O₄, LiCoO₂ and mixed samples with different molar ratios (x).

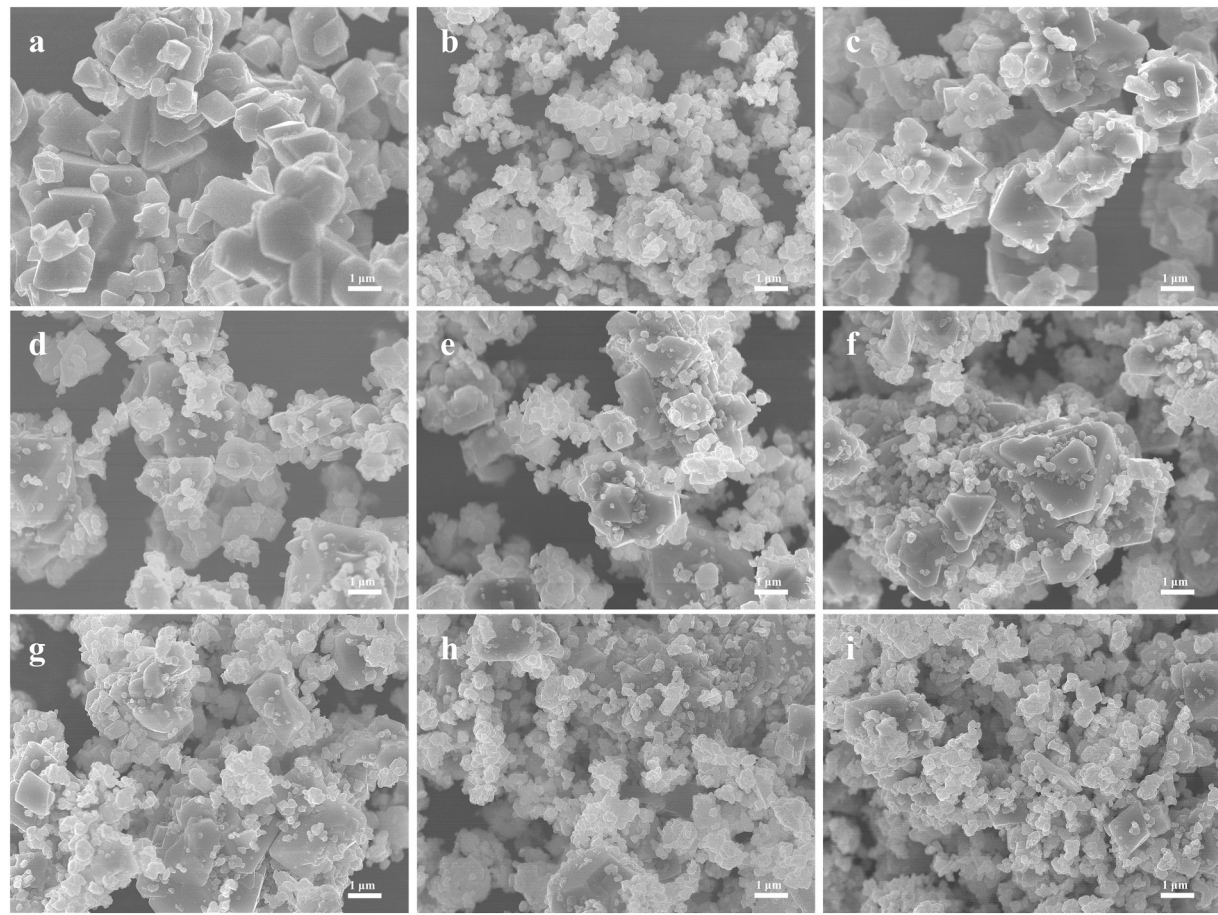


Fig. 2. SEM images of (a) Co_3O_4 , (b) LiCoO_2 and mixed samples with molar ratios of (c) $x = 0.1$, (d) $x = 0.2$, (e) $x = 0.3$, (f) $x = 0.4$, (g) $x = 0.5$, (h) $x = 0.6$, and (i) $x = 0.7$.

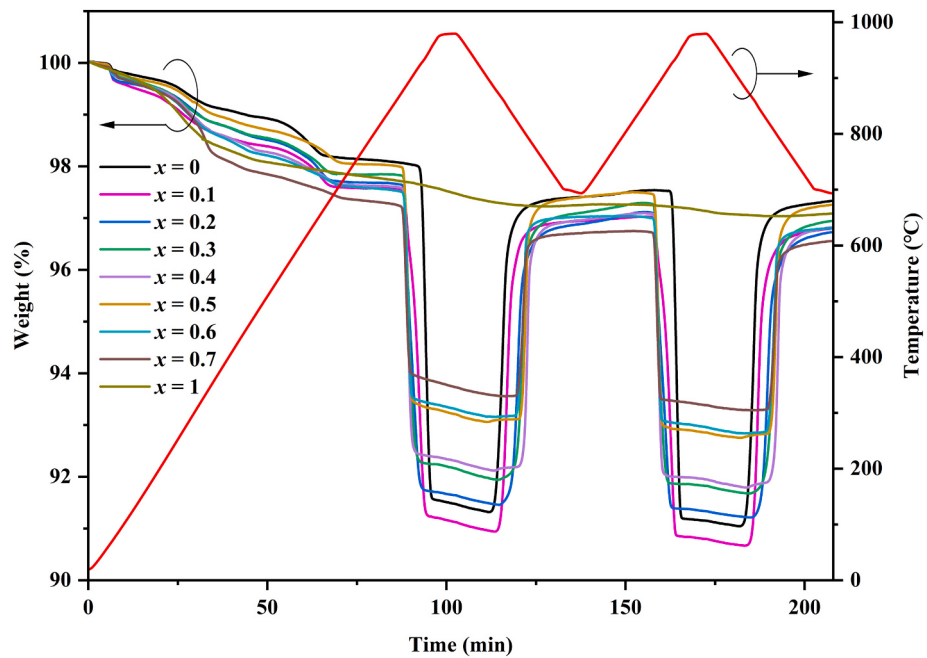


Fig. 3. Thermogravimetric curves of samples with different molar ratios (x).

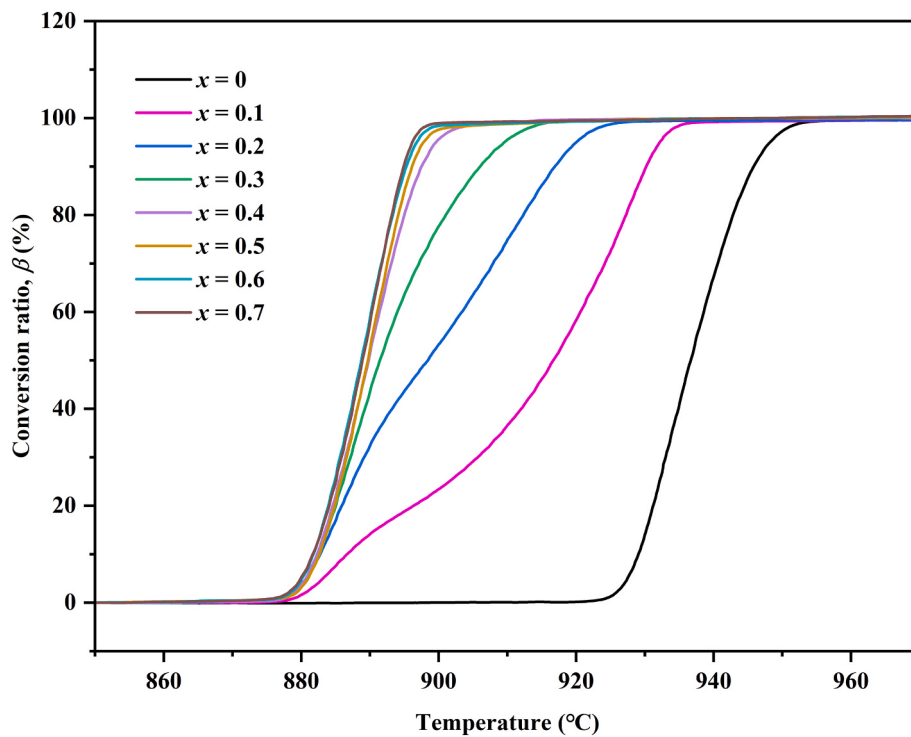


Fig. 4. Reduction profiles for samples with different molar ratios (x).

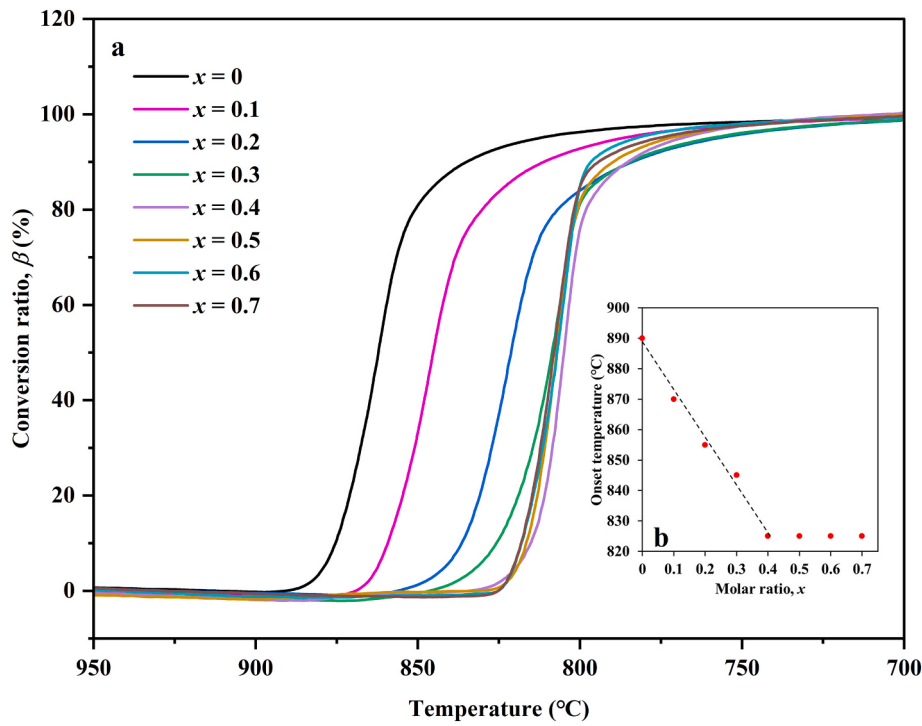


Fig. 5. (a) Re-oxidation profiles for samples with different molar ratios (x) and (b) Evolution of the onset re-oxidation temperature as a function of molar ratio (x).

decreased with increasing doping amount of LiCoO_2 (i.e., with increasing molar ratios (x)). The weight loss upon reduction was nearly $\alpha = 6.5\%$ and the main weight gain upon re-oxidation was nearly $\alpha = 6.3\%$ for pure Co_3O_4 . In the case of mixed samples, the rapid weight loss for the mixed samples with molar ratios of $x = 0.1, 0.2, 0.3, 0.4, 0.5, 0.6$, and 0.7 were nearly $\alpha = 6.4\%, 5.9\%, 5.5\%, 5.2\%, 4.6\%, 4.0\%$, and 3.3% , respectively. Then, in the subsequent re-oxidation process, the

main weight gain for the mixed samples with molar ratios of $x = 0.1, 0.2, 0.3, 0.4, 0.5, 0.6$, and 0.7 were nearly $\alpha = 6.2\%, 5.7\%, 5.3\%, 5.1\%, 4.5\%, 4.0\%$, and 3.3% , respectively. A slight deviation of weight change between reduction and re-oxidation steps occurred for the samples with molar ratios ($x \leq 0.5$). When the molar ratios ($x > 0.5$), the weight recovered completely. As we can observe in Fig. 3, the re-oxidation rate of the samples with molar ratios ($x \leq 0.5$) became relatively low in the

concluding part of re-oxidation process, leading to partial weight gained slowly.

Conversion ratio of reduction and re-oxidation were calculated by eq. (4) from the weight change of each sample in reduction and re-oxidation steps performed by TGA with ramping rates of ± 10 °C/min. Fig. 4 shows the conversion ratio of reduction as a function of temperature during the second cycle for samples with different molar ratios (x). As seen in Fig. 4, the conversion ratio of reduction for each sample increased gradually with increasing temperature. The reduction process of pure Co_3O_4 took place between 925 °C and 955 °C and completed in 3 min. In terms of mixed samples, the reduction process of each mixed sample started at approximately 875 °C, which was lower than that of pure Co_3O_4 . When the molar ratio was $x = 0.1$, the reduction process of the sample took 6.5 min and finished at around 940 °C. With the increasing molar ratios from $x = 0.1$ to 0.4, the reduction rate became faster. When the molar ratio was $x = 0.4$, the reduction process took 3 min and finished at around 905 °C. Then, as we can observe from Fig. 4, similar reduction profiles were exhibited for the mixed samples with molar ratios of $x = 0.4$, 0.5, 0.6, and 0.7. Thus, the mixed sample exhibited an optimum reduction rate when the molar ratio (x) was higher than 0.4. The results reveal that doping with LiCoO_2 contributed to lower the onset temperature of reduction for pure Co_3O_4 . Much more interesting, doping amount of LiCoO_2 was not related to the onset temperature of reduction but impacted on the reduction rate.

Fig. 5a shows the conversion ratio of re-oxidation as a function of temperature during the second cycle for samples with different molar ratios (x). As shown in Fig. 5a, the re-oxidation process of each mixed sample started at a lower temperature in comparison with pure Co_3O_4 . Also, it is worthy to note that the onset temperatures of re-oxidation for mixed samples were obviously different, which differed from the reduction process illustrated in Fig. 4. Furthermore, Fig. 5b illustrates the evolution of the onset temperature of re-oxidation as a function of molar ratio (x). When the molar ratio increased from $x = 0$ to 0.4, the onset temperature of re-oxidation decreased linearly. The onset temperature of re-oxidation for samples with molar ratios of $x = 0$, 0.1, 0.2, 0.3, and 0.4 were approximately 890 °C, 870 °C, 855 °C, 845 °C and 825 °C, respectively. And then, the onset temperature was constant at 825 °C when the molar ratio increased from $x = 0.4$ to 0.7. As shown in Fig. 5a, the conversion ratio of re-oxidation for each sample increased gradually with decreasing temperature. The conversion ratio of pure Co_3O_4 reached nearly $\beta = 95\%$ in 8.5 min when the temperature decreased from 890 °C to 805 °C. Afterwards, the concluding part of the re-oxidation took place slowly in a wide temperature range. When the molar ratio was $x = 0.1$, the conversion ratio for the mixed sample reached nearly $\beta = 95\%$ in 8.5 min with decreasing temperature from 870 °C to 785 °C. Similarly, the concluding part for the mixed sample also took place slowly. With increasing molar ratios from $x = 0.1$ to 0.7, the re-oxidation rate was improved gradually, as shown in Fig. 5a. When the molar ratio was $x = 0.4$, the conversion ratio of the mixed sample reached nearly $\beta = 95\%$ in approximately 6 min with decreasing

temperature from 825 °C to 768 °C. The results illustrated in Fig. 5 indicate that doping with LiCoO_2 leaded to a decrease in the onset temperature of re-oxidation. Moreover, doping amount of LiCoO_2 impacted on the onset temperature of re-oxidation as well as the re-oxidation rate. The onset temperatures of reduction/re-oxidation for samples with different molar ratios (x) were also summarized in Table 1. Accordingly, the optimum molar ratio for the composite was determined as $x = 0.4$ with respective to the onset temperature of reduction/re-oxidation, weight change and reduction/re-oxidation rate.

The effect of LiCoO_2 doping on the redox rate of cobalt oxide was further investigated. Fig. 6 displays the evolution of reduction/re-oxidation conversion ratio as a function of temperature for pure Co_3O_4 sample and the mixed sample with molar ratio of $x = 0.4$ under different heating/cooling rates. As shown in Fig. 6A, the curves of reduction step under different heating rates were nearly identical for the pure Co_3O_4 sample and the mixed sample. While in the case of re-oxidation step, it can be observed that the higher cooling rate exhibited opposite effect on the re-oxidation for pure Co_3O_4 sample and the mixed sample, leading to incomplete conversions for these two samples when the cooling rate was higher than 10 °C/min. Nonetheless, the mixed sample with molar ratio of $x = 0.4$ presented a faster re-oxidation under the higher cooling rate by comparing with pure Co_3O_4 sample, resulting in the higher conversion ratio. As we can see, $\beta = 45\%$ conversion obtained for pure Co_3O_4 sample under the cooling rate of 20 °C/min, while $\beta = 76\%$ conversion obtained for the mixed sample under the same cooling rate. The result indicates that doping with appropriate amount of LiCoO_2 contributed to improve the re-oxidation rate of cobalt oxide-based system under a high cooling rate, which might extend the applicability of the composite in terms of operation conditions. The heat-charging/discharging result was measured by DSC with alumina open crucibles. As shown in Fig. 7, pure Co_3O_4 and the mixed sample both exhibited evident endothermic and exothermic peaks under the heating/cooling rate of 10 °C/min. The ratio between charging and discharging heat for pure Co_3O_4 and the mixed sample were 0.83 and 0.86, respectively. The deviation between charging and discharging heat might attribute to the difference of reaction rate between reduction and re-oxidation processes as well as the heat loss occurred in the open reaction system. When the heating/cooling rate was 20 °C/min, pure Co_3O_4 exhibited a small exothermic peak corresponding to 289.8 kJ/kg, while the mixed sample exhibited a sharp exothermic corresponding to 423.8 kJ/kg. The ratio between charging and discharging heat for pure Co_3O_4 and the mixed sample were 0.46 and 0.74, respectively. The difference in the discharging heat for these two samples under the cooling rate of 20 °C/min may be owing to the different re-oxidation rates as shown in Fig. 6B.

As reported in Fig. 8, the apparent activation energy of reduction for the mixed sample with molar ratio of $x = 0.4$ and pure Co_3O_4 are 435.17 ± 8.39 kJ/mol and 524.85 ± 54.64 kJ/mol, respectively. Meanwhile, the apparent activation energy of oxidation for the mixed sample with molar ratio of $x = 0.4$ and pure Co_3O_4 are 173.88 ± 16.11 kJ/mol and 265.78 ± 19.49 kJ/mol, respectively. By doping with LiCoO_2 , the apparent activation energy of reduction and oxidation were decreased. The result indicates that doping with LiCoO_2 can make reduction and oxidation of cobalt oxide occur more easily.

3.3. Reduction/re-oxidation process exploration

To understand deeply about the effect of LiCoO_2 on the reduction/re-oxidation process of cobalt oxide, in-situ XRD was utilized to explore the process. Fig. 9 (A-D) shows the in-situ XRD patterns of the mixed sample with molar ratio of $x = 0.4$. Fig. 9A shows the XRD patterns in the heating step, as we can observe, the sample exhibited both LiCoO_2 phase (PDF: 01-070-2685) and Co_3O_4 phase (PDF: 00-043-1003) clearly at room temperature. When temperature was higher than 850 °C, the intensity of diffraction peaks decreased with the increasing temperature. Ultimately, the XRD patterns at 950 °C exhibited a single phase of CoO (PDF: 01-076-3829). This behavior demonstrates that both Co_3O_4 and

Table 1

The onset temperature of reduction/re-oxidation and weight change of samples with different molar ratios (x).

Sample	$T_{\text{onset red}}$ (°C) ^a	$T_{\text{onset oxi}}$ (°C) ^a	Weight loss (%) ^b	Weight gain (%) ^b
$x = 0$	925	890	6.5	6.3
$x = 0.1$	875	870	6.4	6.2
$x = 0.2$	875	855	5.9	5.7
$x = 0.3$	875	845	5.5	5.3
$x = 0.4$	875	825	5.2	5.1
$x = 0.5$	875	825	4.6	4.5
$x = 0.6$	875	825	4.0	4.0
$x = 0.7$	875	825	3.3	3.3

^a The onset temperature in this work corresponds to the start temperature of sharp weight change under the configured temperature program.

^b The data of weight loss obtained from the second cycle.

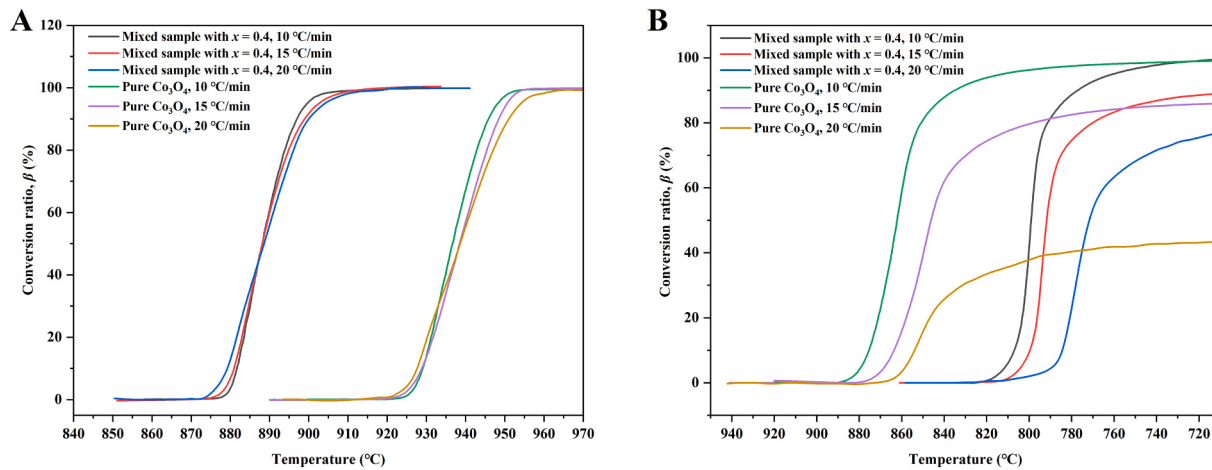


Fig. 6. (A) Reduction and (B) Re-oxidation profiles for pure Co_3O_4 sample and the mixed sample with molar ratio of $x = 0.4$ under different heating/cooling rates.

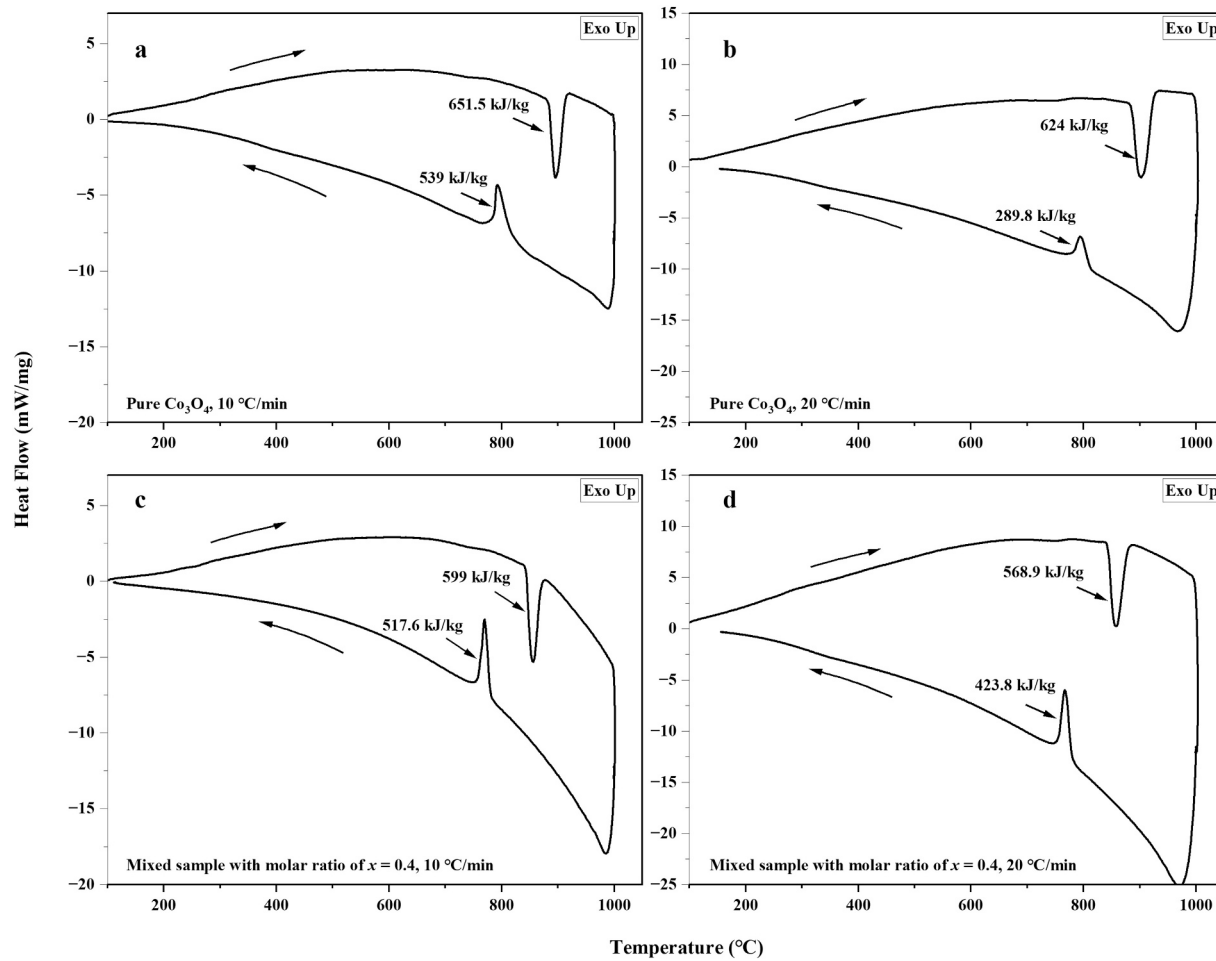


Fig. 7. DSC curves of pure Co_3O_4 and the mixed sample with molar ratio of $x = 0.4$ under different heating/cooling rates: (a) pure Co_3O_4 , 10 $^{\circ}\text{C}/\text{min}$, (b) pure Co_3O_4 , 20 $^{\circ}\text{C}/\text{min}$, (c) the mixed sample with molar ratio of $x = 0.4$, 10 $^{\circ}\text{C}/\text{min}$, and (d) the mixed sample with molar ratio of $x = 0.4$, 20 $^{\circ}\text{C}/\text{min}$.

LiCoO_2 were converted into CoO . It seemed that the Li species inserted into the CoO lattice and formed a CoO -based solid solution. The in-situ XRD patterns shown in Fig. 9B illustrates the re-oxidation process in the cooling step. As we can observe, LiCoO_2 phase and Co_3O_4 phase reproduced while the CoO phase vanished with the decreasing temperature. It should be noted that the structure is detected by in-situ XRD only when the amount of the material is enough. Consequently, no CoO phase was

tested by in-situ XRD when the temperature decreased to 800 $^{\circ}\text{C}$, which differed from the result illustrated in Fig. 5 obtained by TGA. The important matter verified by in-situ XRD is that LiCoO_2 was involved in the reduction/re-oxidation process.

Fig. 9C shows the localized in-situ XRD patterns within the 2 θ range from 17.5° to 20° in the heating step. The diffraction peak corresponding to the LiCoO_2 (003) facets shifted from 18.92° at 30 $^{\circ}\text{C}$ to 18.42° at

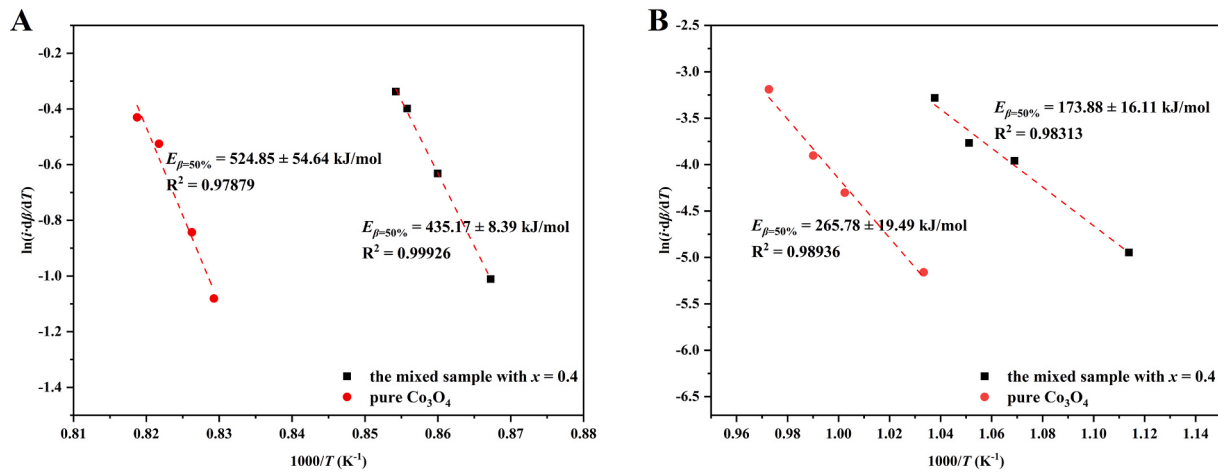


Fig. 8. Isoconversional plots calculated by Friedman method for the (A) reduction and (B) oxidation in air ($\beta = 50\%$).

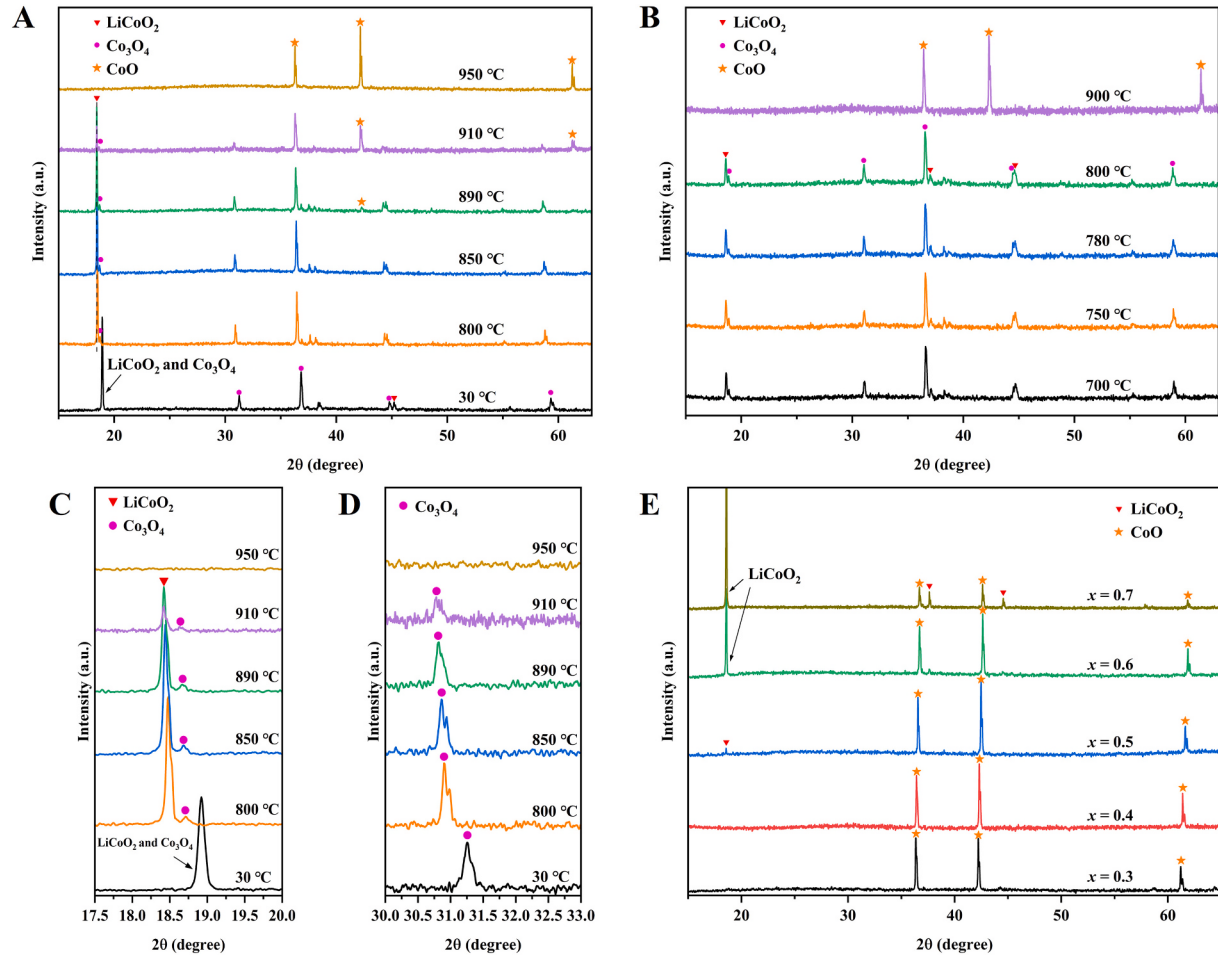


Fig. 9. In-situ XRD patterns of the mixed sample with molar ratio of $x = 0.4$: (A) In the heating step, (B) In the cooling step, (C) Localized XRD patterns within the 2θ range from 17.5° to 20° in the heating step, and (D) Localized XRD patterns within the 2θ range from 30° to 33° in the heating step. And (E) in-situ XRD patterns of mixed samples with different molar ratios (x) at 950 °C.

890 °C, corresponding to an increase in layer spacing of LiCoO_2 from 4.69 Å to 4.81 Å. Similarly, Fig. 9D shows the localized in-situ XRD patterns within the 2θ range from 30° to 33° in the heating step. The diffraction peak, corresponding to the Co_3O_4 (220) facets where present abundant of Co^{3+} [53,54], shifted from 31.26° at 30 °C to 30.82° at 890 °C, corresponding to an increase in the relevant lattice spacing of

Co_3O_4 from 2.86 Å to 2.90 Å. In addition, as we can observe from Fig. 9A, other diffraction peaks of LiCoO_2 phase and Co_3O_4 phase also shifted toward the lower angle side. This behavior means that other facets of LiCoO_2 and Co_3O_4 crystals also expended in the heating step.

Fig. 9E shows the in-situ XRD patterns of mixed samples with different molar ratios (x) at 950 °C and Table 2 shows the lattice

Table 2

Lattice parameters of CoO phase at 950 °C for mixed sample with different molar ratios (x).

Mixed sample	$x = 0.3$	$x = 0.4$	$x = 0.5$	$x = 0.6$	$x = 0.7$
Lattice parameter (Å) ^a	4.28	4.27	4.25	4.24	4.24

^a Lattice parameter is derived from (111) (200) (220) facets based on in-situ XRD analysis.

parameter of the CoO phase at 950 °C for these samples. A single CoO phase (PDF: 01–076-3829) was detected for the mixed samples with molar ratios of $x = 0.3$ and 0.4. When the molar ratio was $x \geq 0.5$, a secondary phase corresponding to LiCoO₂ phase (PDF: 01–070–2685) can be observed. Meanwhile, the lattice parameter of CoO decreased from 4.28 Å to 4.24 Å when the molar ratio (x) increased from 0.3 to 0.6, which might be due to the insertion of Li species (Fig. S1). Afterwards, the lattice parameter was constant when the molar ratio was $x \geq 0.6$. The result indicates that the amount of Li species in the CoO structure increased with the increasing of LiCoO₂ doping amount. Nonetheless, the amount of Li species in CoO structure was limited. This result might account for the different onset temperatures of re-oxidation for mixed samples with different molar ratios (x), as illustrated in Fig. 5 of Section 3.2. With an increase in the doping amount of Li species in CoO lattice, the onset temperature of re-oxidation decreased gradually.

Combined the in-situ XRD results with the redox behaviors discussed in Section 3.2, a plausible reduction/re-oxidation process of the LiCoO₂-doped cobalt oxide composite was proposed, as shown in Fig. 10. In heating step, the lattices of LiCoO₂ and Co₃O₄ slightly expanded with increasing temperature. It is known that lithium ions will extract from or insert into the layered cobalt dioxide matrix of LiCoO₂ by varying the interlayer distance [35–37]. Thus, partial lithium ions extracted from the layered cobalt dioxide matrix when the interlayer distance of LiCoO₂ increased from 4.69 Å to 4.81 Å (De-lithiation process). Simultaneously, the extracted lithium ions inserted into Co₃O₄ lattice, which may render the Co₃O₄ crystal more fragile and stimulate the reduction of Co₃O₄ to start at lower temperature, as discussed in Fig. 4 of Section 3.2. Ultimately, LiCoO₂ and Co₃O₄ converted into CoO-based solid solution. In cooling step, the reverse oxidation process occurred. The CoO-based

solid solution converted to LiCoO₂ and Co₃O₄ in relatively low temperature, which may be owing to the doping lithium ions in CoO lattice. At the same time, the lithium ions inserted into the layered cobalt dioxide matrix of LiCoO₂ (Lithiation process). We assumed the insertion of lithium into Co₃O₄/CoO has a positive effect on the reduction/re-oxidation process. As a further issue, deeper investigation is necessary and required.

3.4. Repeatability test

To examine the repeatability of the composite. The mixed sample with molar ratio of $x = 0.4$, which exhibited an optimum redox behavior, was subjected to 30 runs of reduction/re-oxidation by TGA under an appropriate temperature range. Fig. 11 shows the TGA result of the subjected sample with 30 runs of reduction/re-oxidation. $\alpha = 5.2\%$ weight lost and $\alpha = 5.1\%$ weight recovered in the second cycle, and $\alpha = 5.2\%$ weight lost and $\alpha = 5.2\%$ weight recovered in the 30th cycle. This result demonstrates the feasibility of this composite for TCS application as it can be reused for several cycles. Fig. 12 displays the relevant SEM images of the mixed sample with molar ratio of $x = 0.4$. It can be observed that remarkable changes occurred in the morphology of the sample during reduction/re-oxidation cycles. Differing from the as-prepared sample, the used samples presented coral-like morphologies caused by thermal sintering. Moreover, LiCoO₂ particles could not be distinguished from the bulk. As we can observe from the image taken after 2 cycles, the necks with diameter of around 1 μm formed between the neighboring particles. Meanwhile, open macro-pores presented among the necks. Further, the relatively long necks and large pores shown in the image taken after 30 cycles indicates that there was a further sintering occurred during the subsequent reduction/re-oxidation cycles. The large pores among coral-like structures maybe beneficial to the diffusion of oxygen and facilitate the re-oxidation.

4. Conclusion

In summary, LiCoO₂-doped cobalt oxide composite was proposed and explored for thermochemical energy storage application. The

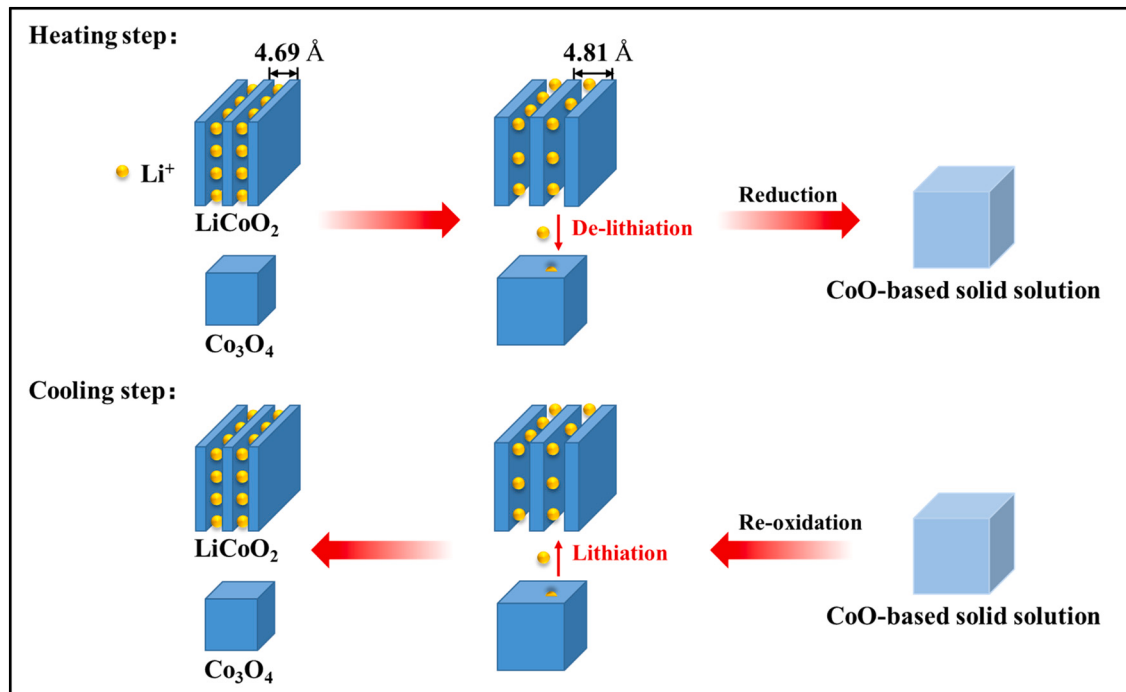


Fig. 10. Plausible reduction/re-oxidation process of LiCoO₂-doped cobalt oxide composite.

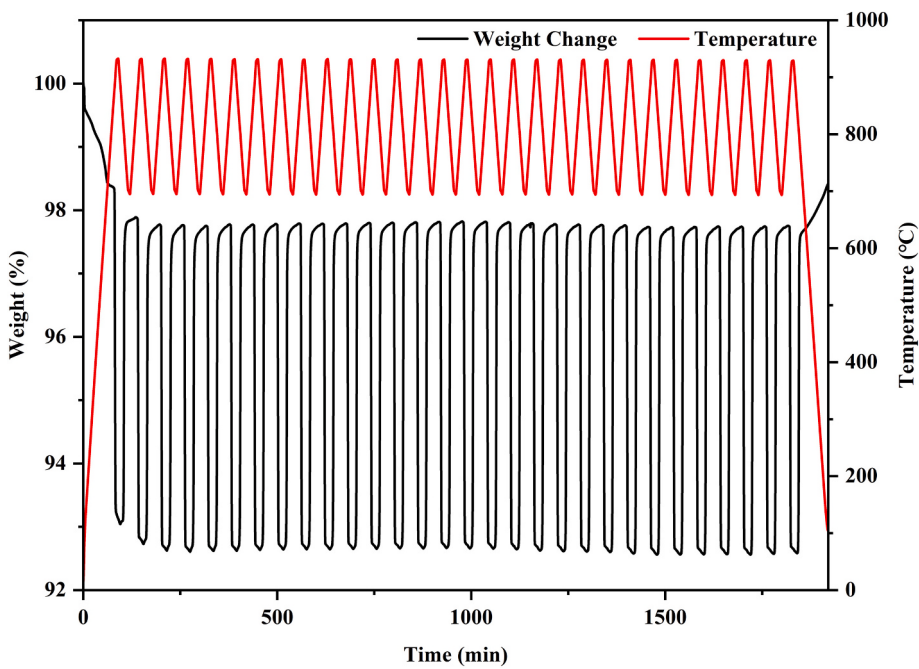


Fig. 11. Thermogravimetric curve of the mixed sample with molar ratio of $x = 0.4$ under 30 runs of reduction/re-oxidation.

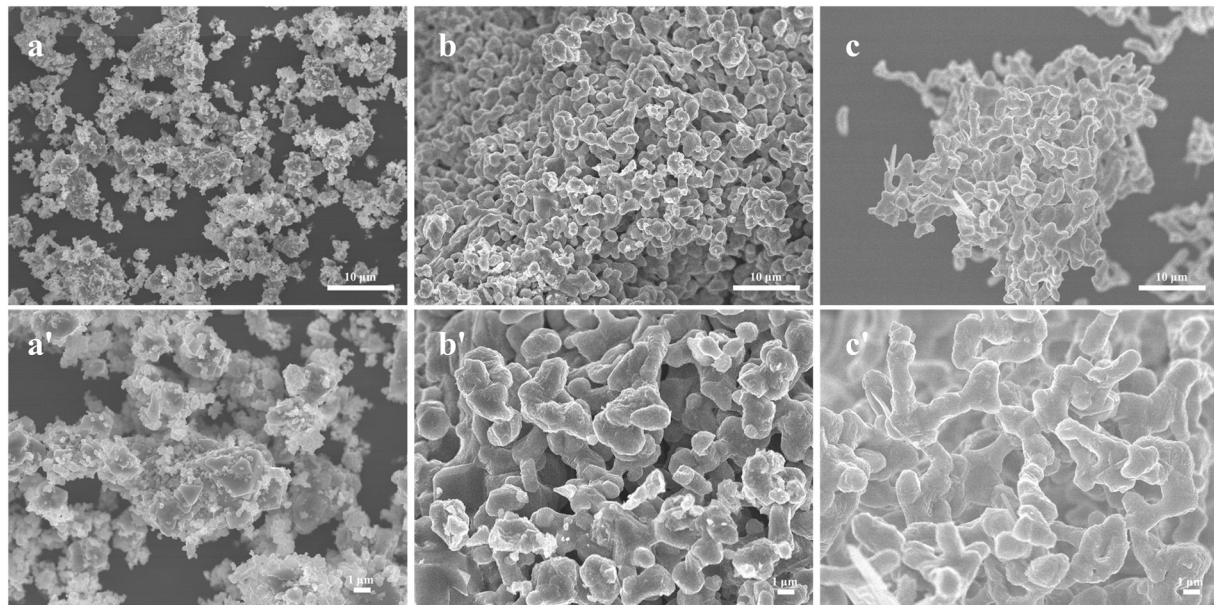


Fig. 12. SEM images of the mixed sample with molar ratio of $x = 0.4$: (a and a') as-prepared sample, (b and b') after 2 cycles, and (c and c') after 30 cycles.

composite was facilely obtained by physical mixing process, which is advantageous to scale-up research and practical application.

The reduction/re-oxidation behavior of LiCoO₂-doped cobalt oxide composite was investigated. The optimum doping amount of LiCoO₂ in composite was determined by the reduction/re-oxidation temperature, weight change and reduction/re-oxidation rate. It was found that doping with LiCoO₂ diminished the onset temperature of reduction and re-oxidation by 50 °C and 65 °C, respectively. Also, doping with appropriate amount of LiCoO₂ contributed to improve the re-oxidation rate of cobalt oxide-based system under a high cooling rate, resulting the discharging heat (423.8 kJ/kg) increased significantly in comparison with pure cobalt oxide (289.8 kJ/kg) under temperature cooling rate of 20 °C/min. Doping with LiCoO₂ was found to decrease the apparent

activation energy of reduction and oxidation. Meanwhile, excellent repeatability of this composite was attested in 30 cycles. Hence, LiCoO₂-doped cobalt oxide was proved as a promising candidate for TCS application. Moreover, the in-situ XRD results demonstrated that LiCoO₂ was involved in the reduction/re-oxidation process. The effect of lithium ions on the reduction/re-oxidation process would be investigated in the future. In addition, as doping with lithium compounds has been verified as an effective method to expanding the possibility of metal oxides for TCS application, more lithium compounds and metal oxide pairs would be tested in the future.

CRediT authorship contribution statement

Rongjun Wu: Conceptualization, Methodology, Investigation, Writing – original draft. **Lisheng Deng:** Investigation. **Hongyu Huang:** Resources, Writing – review & editing. **Mitsuhiro Kubota:** Resources. **Noriyuki Kobayashi:** Supervision.

Declaration of competing interest

The authors declare that they have no known competing financial interests or personal relationships that could have appeared to influence the work reported in this paper.

Data availability

Data will be made available on request.

Acknowledgements

This work was partially supported by “Knowledge Hub Aichi”, Priority Research Project from Aichi Prefectural Government, Japan and the National Natural Science Foundation of China (No.52176091).

Appendix A. Supplementary data

Supplementary data to this article can be found online at <https://doi.org/10.1016/j.est.2022.105774>.

References

- [1] H. Mahon, D. O'Connor, D. Friedrich, B. Hughes, A review of thermal energy storage technologies for seasonal loops, *Energy* 239 (2022), 122207.
- [2] S. Kuravi, J. Trahan, D. Yogi Goswami, M.M. Rahman, E.K. Stefanakos, Thermal energy storage technologies and systems for concentrating solar power plants, *Prog. Energy Combust. Sci.* 39 (2013) 285–319.
- [3] L. André, S. Abanades, G. Flamant, Screening of thermochemical systems based on solid-gas reversible reactions for high temperature solar thermal energy storage, *Renew. Sustain. Energy Rev.* 64 (2016) 703–715.
- [4] A.J. Carrillo, J. González-Aguilar, M. Romero, J.M. Coronado, Solar energy on demand: a review on high temperature thermochemical heat storage systems and materials, *Chem. Rev.* 119 (2019) 4777–4816.
- [5] X. Yang, S. Li, J. Zhao, X. Wang, H. Huang, Y. Wang, Construction of metal organic framework-derived hollow-structured mesoporous carbon based lithium hydroxide composites for low-grade thermal energy storage, *Compos. Part B* 232 (2022), 109604.
- [6] A. Bayon, R. Bader, M. Jafarian, L. Fedunik-Hofman, Y. Sun, J. Hinkley, S. Miller, W. Lipinski, Techno-economic assessment of solid-gas thermochemical energy storage systems for solar thermal power applications, *Energy* 149 (2018) 473–484.
- [7] A.J. Carrillo, D. Sastre, D.P. Serrano, P. Pizarro, J.M. Coronado, Revisiting the BaO₂/BaO redox cycle for solar thermochemical energy storage, *Phys. Chem. Chem. Phys.* 18 (2016) 8039–8048.
- [8] K.N. Hutchings, M. Wilson, P.A. Larsen, R.A. Cutler, Kinetic and thermodynamic considerations for oxygen absorption/desorption using cobalt oxide, *Solid State Ionics* 177 (2006) 45–51.
- [9] C. Agrafiotis, M. Roeb, M. Schmücker, C. Sattler, Exploitation of thermochemical cycles based on solid oxide redox systems for thermochemical storage of solar heat. Part 1: testing of cobalt oxide-based powders, *Sol. Energy* 102 (2014) 189–211.
- [10] C. Agrafiotis, M. Roeb, M. Schmücker, C. Sattler, Exploitation of thermochemical cycles based on solid oxide redox systems for thermochemical storage of solar heat. Part 2: redox oxide-coated porous ceramic structures as integrated thermochemical reactors/heat exchangers, *Sol. Energy* 114 (2015) 440–458.
- [11] C. Agrafiotis, S. Tescari, M. Roeb, M. Schmücker, C. Sattler, Exploitation of thermochemical cycles based on solid oxide redox systems for thermochemical storage of solar heat. Part 3: cobalt oxide monolithic porous structures as integrated thermochemical reactors/heat exchangers, *Sol. Energy* 114 (2015) 459–475.
- [12] C. Agrafiotis, M. Roeb, C. Sattler, Exploitation of thermochemical cycles based on solid oxide redox systems for thermochemical storage of solar heat. Part 4: screening of oxides for use in cascaded thermochemical storage concepts, *Sol. Energy* 139 (2016) 695–710.
- [13] A.J. Carrillo, D.P. Serrano, P. Pizarro, J.M. Coronado, Thermochemical heat storage based on the Mn₂O₃/Mn₃O₄ redox couple: influence of the initial particle size on the morphological evolution and cyclability, *J. Mater. Chem. A* 2 (2014) 19435–19443.
- [14] E. Alonso, C. Pérez-Rábago, J. Licurgo, E. Fuentealba, C.A. Estrada, First experimental studies of solar redox reactions of copper oxides for thermochemical energy storage, *Sol. Energy* 115 (2015) 297–305.
- [15] S.M. Babiniec, E.N. Coker, J.E. Miller, A. Ambrosini, Investigation of LaxSr_{1-x}CoyM_{1-y}O_{3-δ} (M = Mn, Fe) perovskite materials as thermochemical energy storage media, *Solid Energy* 118 (2015) 451–459.
- [16] K.J. Albrecht, G.S. Jackson, R.J. Braun, Thermodynamically consistent modeling of redox-stable perovskite oxides for thermochemical energy conversion and storage, *Appl. Energy* 165 (2016) 285–296.
- [17] Z. Zhang, L. Andre, S. Abanades, Experimental assessment of oxygen exchange capacity and thermochemical redox cycle behavior of Ba and Sr series perovskites for solar energy storage, *Sol. Energy* 134 (2016) 494–502.
- [18] N. Gokon, T. Yawata, S. Bellan, T. Kodama, H.-S. Cho, Thermochemical behavior of perovskite oxides based on LaxSr_{1-x}(Mn, Fe, Co)O_{3-δ} and Ba_xY_{1-x}CoO_{3-δ} redox system for thermochemical energy storage at high temperatures, *Energy* 171 (2019) 971–980.
- [19] A.J. Carrillo, D.P. Serrano, P. Pizarro, J.M. Coronado, Improving the thermochemical energy storage performance of the Mn₂O₃/Mn₃O₄ redox couple by the incorporation of iron, *ChemSusChem* 8 (2015) 1947–1954.
- [20] A.J. Carrillo, D.P. Serrano, P. Pizarro, J.M. Coronado, Understanding redox kinetics of iron-doped manganese oxides for high temperature thermochemical energy storage, *J. Phys. Chem. C* 120 (2016) 27800–27812.
- [21] L. André, S. Abanades, L. Cassayre, High-temperature thermochemical energy storage based on redox reactions using Co-Fe and Mn-Fe mixed metal oxides, *J. Solid State Chem.* 253 (2017) 6–14.
- [22] C. Agrafiotis, T. Block, M. Senholdt, S. Tescari, M. Roeb, C. Sattler, Exploitation of thermochemical cycles based on solid oxide redox systems for thermochemical storage of solar heat. Part 6: testing of Mn-based combined oxides and porous structure, *Sol. Energy* 149 (2017) 227–244.
- [23] A.J. Carrillo, D.P. Serrano, P. Pizarro, J.M. Coronado, Manganese oxide-based thermochemical energy storage: modulating temperatures of redox cycles by Fe-Cu Co-doping, *J. Energy Storage* 5 (2016) 169–176.
- [24] T. Block, M. Schmücker, Metal oxides for thermochemical energy storage: a comparison of several metal oxide systems, *Sol. Energy* 126 (2016) 195–207.
- [25] F. Varsano, C. Alvani, A.L. Barbera, A. Masi, F. Padella, Lithium manganese oxides as high-temperature thermal energy storage system, *Thermochim. Acta* 640 (2016) 26–35.
- [26] N.W. Hlongwa, D. Sastre, E. Iwuoha, A.J. Carrillo, C. Ikpo, D.P. Serrano, P. Pizarro, J.M. Coronado, Exploring the thermochemical heat storage capacity of AMn₂O₄ (A = Li or Cu) spinels, *Solid State Ionics* 320 (2018) 316–324.
- [27] A. Waris, M. Din, A. Ali, S. Afzidi, A. Baset, A.U. Khan, M. Ali, Green fabrication of Co and Co₃O₄ nanoparticles and their biomedical applications: a review, *OpenLife Sci.* 16 (2021) 14–30.
- [28] Y. Lyu, X. Wu, K. Wang, Z. Feng, T. Cheng, Y. Liu, M. Wang, R. Chen, L. Xu, J. Zhou, Y. Lu, B. Guo, An overview on the advances of LiCoO₂ cathodes for lithium-ion batteries, *Adv. Energy Mater.* 11 (2021) 2000982–2001010.
- [29] T.-R. Kuo, W.-T. Chen, H.-J. Liao, Y.-H. Yang, H.-C. Yen, T.-W. Liao, C.-Y. Wen, Y.-C. Lee, C.-C. Chen, D.-Y. Wang, Improving hydrogen evolution activity of earth-abundant cobalt-doped iron pyrite catalysts by surface modification with phosphide, *Small* 13 (2017) 1603356–1603361.
- [30] T.-Y. Chen, T.-R. Kuo, S. Yougbaré, L.-Y. Lin, C.-Y. Xiao, Novel direct growth of ZIF-67 derived Co₃O₄ and N-doped carbon composites on carbon cloth as supercapacitor electrodes, *J. Colloid Interface Sci.* 608 (2022) 493–503.
- [31] B. Wong, in: *Thermochemical Heat Storage for Concentrated Solar Power*, Final Report for the U.S. Department of Energy, United States, 2011, pp. 10–31.
- [32] T. Block, N. Knoblauch, M. Schmücker, The cobalt-oxide/iron-oxide binary system for use as high temperature thermochemical energy storage material, *Thermochim. Acta* 577 (2014) 25–32.
- [33] A.J. Carrillo, J. Moya, A. Bayón, P. Jana, V.A. de la Peña O’Shea, M. Romero, J. González-Aguilar, D.P. Serrano, P. Pizarro, J.M. Coronado, Thermochemical energy storage at high temperature via redox cycles of Mn and Co oxides: pure oxides versus mixed ones, *Sol. Energy Mater. Sol. Cells* 123 (2014) 47–57.
- [34] Y. Portilla-Nieto, A. Zaki, K. Vidal, M. Hernaiz, A. Aranzabe, S. Doppiu, A. Faik, Development of Co_{3-x}Ni_xO₄ materials for thermochemical energy storage at lower red-ox temperature, *Sol. Energy Mater. Sol. Cells* 230 (2021) 111194.
- [35] T. Ohzuku, A. Ueda, Solid-state redox reactions of LiCoO₂ (R3m) for 4 volt secondary lithium cells, *J. Electrochem. Soc.* 141 (1994) 2972.
- [36] H. Wang, S. Xu, C. Tsai, Y. Li, C. Liu, J. Zhao, Y. Liu, H. Yuan, F. Abild-Pedersen, F. B. Prinz, J.K. Nørskov, Y. Cui, Direct and continuous strain control of catalysts with tunable battery electrode materials, *Science* 354 (2016) 1031–1036.
- [37] Z. Lu, G. Chen, Y. Li, H. Wang, J. Xie, L. Liao, C. Liu, Y. Liu, T. Wu, Y. Li, A.C. Luntz, M. Bajdich, Y. Cui, Identifying the active surfaces of electrochemically tuned LiCoO₂ for oxygen evolution reaction, *J. Am. Chem. Soc.* 139 (2017) 6270–6276.
- [38] P.E. Marín, Y. Milian, S. Ushak, L.F. Cabeza, M. Grágeda, G.S.F. Shire, Lithium compounds for thermochemical energy storage: a state-of-the-art review and future trends, *Renew. Sustain. Energy Rev.* 149 (2021), 111381.
- [39] J. Yan, C.Y. Zhao, First-principle study of CaO/Ca(OH)₂ thermochemical energy storage system by Li or Mg cation doping, *Chem. Eng. Sci.* 117 (2014) 293–300.
- [40] J. Ryu, N. Hirao, R. Takahashi, Y. Kato, Dehydration behavior of metal-salt-added magnesium hydroxide as chemical heat storage media, *Chem. Lett.* 37 (2008) 1140.
- [41] H. Ishitobi, N. Hirao, J. Ryu, Y. Kato, Evaluation of heat output densities of lithium chloride-modified magnesium hydroxide for thermochemical energy storage, *Ind. Eng. Chem. Res.* 52 (2013) 5321–5325.
- [42] O. Myagmarjav, J. Ryu, Y. Kato, Lithium bromide-mediated reaction performance enhancement of a chemical heat-storage material for magnesium oxide/water chemical heat pumps, *Appl. Therm. Eng.* 63 (2014) 170–176.

- [43] A. Shkatulov, Y. Aristov, Modification of magnesium and calcium hydroxides with salts: an efficient way to advanced materials for storage of middle-temperature heat, *Energy* 85 (2015) 667–676.
- [44] A.I. Shkatulov, Y. Aristov, Thermochemical energy storage using LiNO₃-doped Mg(OH)₂: a dehydration study, *Energy Technol.* 6 (2018) 1844–1851.
- [45] A. Shkatulov, H. Takasu, Y. Kato, Y. Aristov, Thermochemical energy storage by LiNO₃-doped Mg(OH)₂: rehydration study, *J. Energy Storage* 22 (2019) 302–310.
- [46] S. Li, J. Liu, T. Tan, J. Nie, H. Zhang, Optimization of LiNO₃-Mg(OH)₂ composites as thermo-chemical energy storage materials, *J. Environ. Manag.* 262 (2020), 110258.
- [47] A. Maruyama, R. Kurosawa, J. Ryu, Effect of lithium compound addition on the dehydration and hydration of calcium hydroxide as a chemical heat storage material, *ACS Omega* 5 (2020) 9820–9829.
- [48] A.I. Shkatulov, S.T. Kim, H. Miura, Y. Kato, Y.I. Aristov, Adapting the MgO-CO₂ working pair for thermochemical energy storage by doping with salts, *Energy Convers. Manag.* 185 (2019) 473–481.
- [49] S. Vyazovkin, A.K. Burnham, J.M. Criado, L.A. Perez-Maqueda, ICTAC kinetics committee recommendations for performing kinetic computations on thermal analysis data, *Thermochim. Acta* 520 (2011) 1–19.
- [50] H.L. Friedman, Kinetics of thermal degradation of char-forming plastics from thermogravimetry. Application to a phenolic plastic, *J. Polym. Sci. C* 6 (1964) 183–195.
- [51] X. Shi, H. Zheng, A.M. Kannan, K. Pérez-Salcedo, B. Escobar, Effect of thermally induced oxygen vacancy of α -MnO₂ nanorods toward oxygen reduction reaction, *Inorg. Chem.* 58 (2019) 5335–5344.
- [52] G. Zhuang, Y. Chen, Z. Zhuang, Y. Yu, J. Yu, Oxygen vacancies in metal oxides: recent progress towards advanced catalyst design, *Sci. China Mater.* 63 (2020) 2089–2118.
- [53] X. Xie, Y. Li, Z.Q. Liu, M. Haruta, W. Shen, Low-temperature oxidation of CO catalysed by Co₃O₄ nanorods, *Nature* 458 (2009) 746.
- [54] Y. Zhang, F. Ding, C. Deng, S. Zhen, X. Li, Y. Xue, Y.M. Yan, K. Sun, Crystal plane-dependent electrocatalytic activity of Co₃O₄ toward oxygen evolution reaction, *Catal. Commun.* 67 (2015) 78–82.